New Journal of Physics
The open access journal for physics

Transmission of surface plasmon polaritons through atomic-size constrictions

D Benner, J Boneberg, P Nürnberger, G Ghafoori, P Leiderer and E Scheer[1]

University of Konstanz, Universitätsstraße 10, D-78464 Konstanz, Germany
E-mail: elke.scheer@uni-konstanz.de

New Journal of Physics **15** (2013) 113014 (11pp)
Received 24 May 2013
Published 7 November 2013
Online at http://www.njp.org/
doi:10.1088/1367-2630/15/11/113014

Abstract. We study the excitation and propagation of surface plasmon polaritons (SPPs) on a micron-sized thin gold stripe. Grating couplers are embedded for both excitation of SPPs and detection after propagation. The experimental setup allows measuring of the decay length of the SPPs on the gold stripe excited in the near infrared part of the electromagnetic spectrum. We show that SPPs are transmitted with a surprisingly high probability across a tapered constriction, with smallest lateral dimensions of atomic size.

S Online supplementary data available from stacks.iop.org/NJP/15/113014/mmedia

Contents

[1] Author to whom any correspondence should be addressed.

1. Introduction

Plasmonic devices have been proposed to realize particular functionalities in optoelectronic devices, because they promise to overcome the size mismatch between nanometre-sized electronic building blocks and the microscale used in optics and photonics devices [1–3]. Plasmonic devices allow manipulating light on a scale well below its wavelength. One aspect of these devices deals with the transport of surface plasmon polaritons (SPPs) towards a small area for focusing electro-magnetic (em) waves. An em wave with a wavelength of several hundred nanometres in vacuum can be focused down to a few nanometres owing to the bound state of SPPs at a metallic surface [4–7]. Such an application requires a suitable waveguide for the transport of the SPPs towards the desired area [8–13].

The focusing of light to a small area is of utmost importance in nano-optoelectronics, i.e. when addressing ultrasmall electronic building blocks by light. As an example, we name studies of the electron transport through atomic size contacts or molecular junctions under light irradiation. As the few existing experiments have shown till now, the conductance of atomic contacts can be manipulated by SPPs [14–23]. The interpretation of these experiments is hampered by the fact that the SPP intensity transmitted at the atomic contact and across it is not known, because a near-field optical measurement setup cannot easily be integrated into these experiments.

Here, we show an experimental technique which allows measuring SPP transport across a constriction with lateral dimension well below the vacuum light wavelength. The shape of the sample has been chosen in analogy to the mentioned transport experiments, e.g. with the mechanically controlled break junction technique (MCBJ) as reported in [14, 15, 18]. As an additional feature, a grating is engraved that enables the excitation of SPPs. These SPPs propagate along the sample, and further gratings allow converting them back into photons which can be detected in the far field. Thus the transport of SPPs on a metallic stripe and their transmission through a constriction connecting two stripes can be measured [10, 11]. For comparison we performed finite difference time domain (FDTD) simulations solving Maxwell's equations for our sample geometry. Our findings pave the way for the development of optimized metal stripe waveguides for optoelectronic effects in nanocontacts.

2. Experimental methods

2.1. Sample preparation

The suspended nanobridges are fabricated by electron beam lithography. First, polyimide is spin coated (2.5 μm in thickness) onto a softly polished stainless steel wafer (300 μm in thickness). The wafer is annealed for 6 h at 430 °C in vacuum (10^{-5} mbar). The polyimide layer serves as an electrical insulator and a sacrificial layer in the subsequent etching process. The polyimide has a refractive index of typically $n = 1.81$[2]. Prior to performing the electron beam lithography process, the wafer is cut to size ($22 \times 4 \times 0.3\,\mathrm{mm}^3$) and a double layer of electron-beam resists, MMA-MAA/PMMA[3], is deposited by spin coating on the substrate and baked in an oven at 170 °C for 30 min. The electron beam lithography is performed in a scanning

[2] Technical product information FUJIFILM, Polyamic Acid Durimide 100.

[3] Methyl methacrylate (MMA), methacrylic acid (MAA), polymethyl methacrylate (PMMA), isopropyl alcohol (IPA), methyl isobutyl ketone (MIBK).

electron microscope (SEM) operating at 30 kV and equipped with a pattern generator. After being exposed and developed in IPA:MIBK (3:1) (see footnote 3), the patterned samples are mounted in an electron-beam evaporator chamber of ultra-high vacuum (10^{-9} mbar) and gold of 100 nm thickness is deposited at a rate of 1.5 Å s^{-1}. The process is accomplished by lifting off the mask in isopropanol. The total length of the structure is about 70 μm and the width is 4 μm. By design, the length of the constriction is about 2.5 μm and the width varies linearly from 1 μm down to 50 nm. The smallest contact area of the constriction can be estimated from SEM and atomic force microscope (AFM) images to range between 20×20 and $100 \times 100\,\text{nm}^2$ in length and width, respectively. After lift-off, the milling of the gratings is performed with the help of a focused ion beam [24]. The gratings have a period of about 760 nm according to the wavelength of the SPPs at the interface gold/air when illuminating with a laser wavelength of 780 nm under normal incidence. Each trench of the gratings has dimensions of $0.4 \times 3.2 \times 0.09\,\mu\text{m}^3$ in length, width and depth, respectively. As a last step, the polyimide layer is partially etched away (thickness reduction ~700 nm) by employing O_2 plasma in the vacuum chamber of a reactive ion etcher in order to form a free-standing bridge [14, 15].

2.2. Optical setup

For the optical investigation of the sample, we use a microscope setup with a spatial resolution of about 800 nm (see figure S1 in the supplementary data (SD) (available from stacks.iop.org/NJP/15/113014/mmedia)). The pulsed light of a laser diode with time-averaged input power from several to several tens of μW passes the quarter-wave retarder to fine tune the polarization state in order to correct for small changes caused by optical components. The polarization of the electric field of the incoming light is adjusted parallel to the long axis of the stripe by the half-wave retarder. After the 50/50 beam splitter, the light is focused by a lens at normal incidence onto the sample to a spot diameter (full-width at half-maximum) of about 1.7 μm with 35° beam divergence. For controlling the actual position of the laser spot, white light can be coupled into the path by a cold mirror. The spatial distribution of the light intensity from the sample is collected with a CCD camera.

2.3. Finite difference time domain simulations

We used the program package FDTD Solutions from Lumerical. We model a supported gold stripe with partly freestanding constriction and gratings in the same geometrical arrangement as the sample. For the simulation data shown we neglected surface roughness of the gold film. The method to extract the transmission probabilities T_c is analogous to the method for extracting the decay length l. As an example, figure S3 (in the SD) depicts the cross section of the intensity distribution perpendicular to the bare gold stripe for a distance of 9.0 μm (see figure 4(a)). The intensity distribution from the bottom side of the gold stripe up to 800 nm above the gold surface is shown. We read out an intensity averaged over an area of $3 \times 0.85\,\mu\text{m}^2$ in width and height at various distances. These intensities from the cross sections are used to solve the equations given below in the following section.

3. Results and discussion

Along the lines of [25–28], we optimized the grating parameters with the help of FDTD simulations. The calculations were performed for a high SPP excitation efficiency according

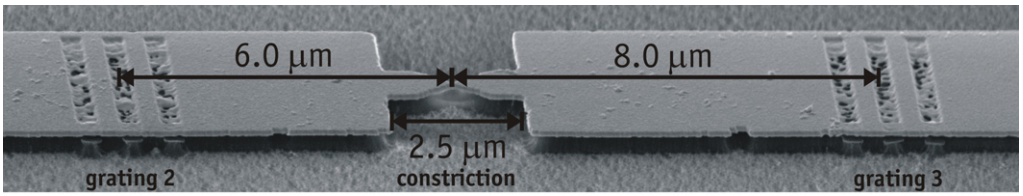

Figure 1. SEM picture of the central part of the gold stripes with the gratings on the left and the right side of the constriction connecting the stripes; the grating period is about 760 nm with trenches of about $0.4 \times 3.2 \times 0.09\,\mu m^3$ in length, width and depth. The distances from the middle of the gratings are about 6.0 and $-8.0\,\mu$m (the minus sign indicates the position at the right side of the constriction). The picture was taken at a tilting angle of 54°.

to the conditions of our optical setup. The distances from the middle of a grating to the centre of the constriction where a metallic point contact (MPC) can be established are about $6.0\,\mu$m (grating 2) and $-8.0\,\mu$m (grating 3). A third one, labelled grating 1, located at $21.6\,\mu$m from the constriction, is not shown in figure 1. For the optical investigation of the sample we use a microscope setup with a spatial resolution of about 800 nm. Pulses of about $2\,\mu$s, with a duty cycle of 1:10, are used. The power ranges from several to several tens of μW. The polarization of the incoming light is adjusted parallel to the long axis of the stripe (for details see SD (available from stacks.iop.org/NJP/15/113014/mmedia)).

At first we discuss the optical characterization of the sample. For that purpose we positioned the laser spot in central position of the stripe and collected the light emitted from the sample with the CCD camera (see figure 2). The strongest feature in the frames is the direct reflection of the illuminating laser beam itself. Even for a position on the unpatterned stripe (see frame at $13\,\mu$m), the reflected light is accompanied by a ring like structure around the central spot arising from diffraction. Besides this signal, we observe no light being emitted from areas close to the constriction and the gratings. In contrast, when illuminating one of the gratings, we clearly observe light being emitted from each of the other optical elements, i.e. the other gratings and the constriction. This light contribution is interpreted as being caused by travelling SPPs that are output coupled as photons preferentially at the optical elements. For example, when illuminating the grating 1 positioned at $21.6\,\mu$m, we detect emitted light at grating 2, at the constriction, and at grating 3 as indicated by the red circles. When irradiating at positions of 6.0 and $-8.0\,\mu$m, the reflected intensity of the laser spot and the emitted intensity at the constriction start to merge, hampering a precise determination of the light emission at the constriction. The power dependence of the outcoupled light as well as the propagation of a running SPP are visualized in supplementary movies 1 and 2 (available at stacks.iop.org/NJP/15/113014/mmedia).

Reflection and diffraction of the exciting laser light result in a non-negligible background signal, as the optical pictures in figure 2 illustrate. In order to deduce the contribution of the SPPs being emitted at the gratings and the constriction, we performed a subtraction method. As the cross sections (red line 1 and blue line 2) in the top panel in figure 3 indicate, the intensity along the long axis of the stripe was analysed in both directions from the excitation point.

The intensity along the cross sections is averaged in perpendicular direction to the long axis of the stripe at a diameter of $3.2\,\mu$m, corresponding to the width of the gratings. At the

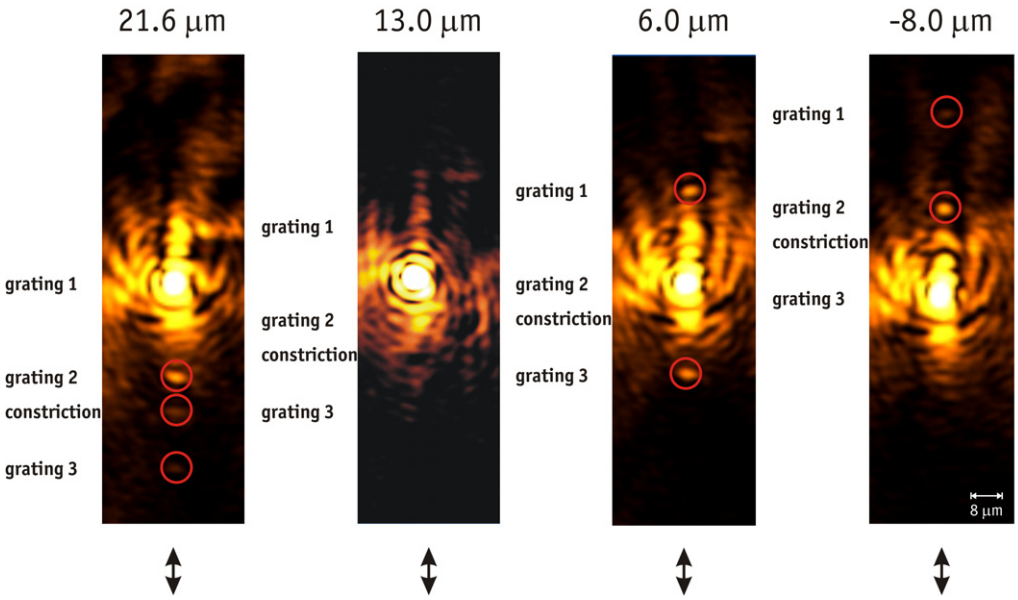

Figure 2. Distribution of the collected light when illuminating the sample at four different positions (image is rotated by 90° compared to figure 1). The brightest intensity distribution results from the back-reflected laser spot and therewith indicates the position of excitation of the SPPs. The red circles mark areas at which the SPPs are emitted into the far field for the light polarization parallel to the orientation of the gold stripe.

side of blue line 2, where no optical element is present, no additional intensity anomalies are observed at the corresponding positions of the optical elements. This signal thus corresponds to the distance-dependent back reflection and diffraction contributions to the total intensity signal. We subtract this intensity from the intensity measured along line 1 and obtain the bare SPP contribution to the emitted intensity. The lower panel of figure 3 shows the original curves and the result of this subtraction method for the illumination of grating 1. The inset corresponding to a blow-up of the dashed box shows the SPP contribution of the gratings and the constriction in a range of 6.0 to $-8.0\,\mu$m. Table 1 summarizes the results and the distance dependences of the emitted light intensities for the excitation at gratings 1 and 3. For that purpose we averaged the emitted intensity along the long axis of the stripe at a length of 1 μm. The results reveal a decrease of intensity for increasing distance between excitation and output coupling as expected for travelling SPPs undergoing decay processes during their travel.

The chosen experimental arrangement allows the determination of optical intensities at different positions. For this purpose we use the following model: at the illuminated grating, SPPs are excited with certain efficiency. From the excitation point the SPPs travel in both directions. On their way they experience an exponential decay with a decay length l. At the next optical element they might be reflected, absorbed, scattered or transmitted. Assuming that all gratings behave similarly, we use the exponential decay between the gratings for determining the transmission probability of the MPC as follows. When illuminating at grating 3, the ratio between the intensities measured at gratings 1 and 2 should be described by the following

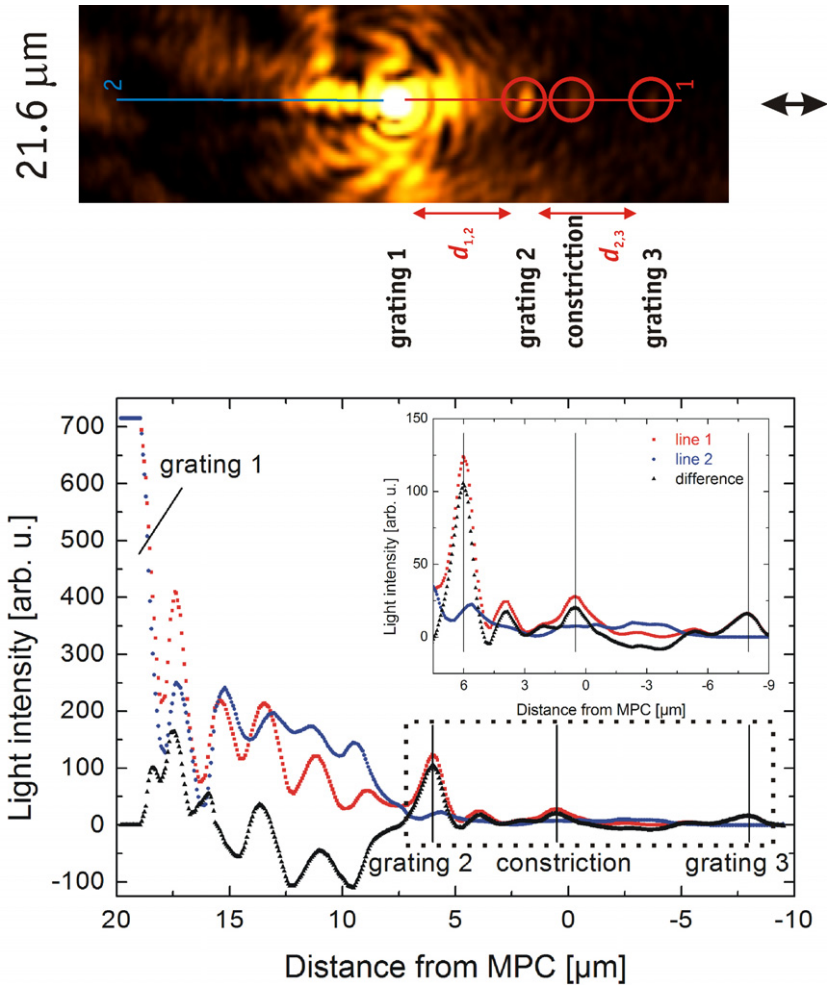

Figure 3. Top panel: distribution of the back-reflected light when illuminating the sample at grating 1 (see also figure 2). The lines 1 (red) and 2 (blue) indicate cross sections along the long axis of the stripe. The red circles mark areas at which the SPPs are emitted into the far field. Bottom panel: intensity cross sections from the top panel and resulting difference curve obtained by subtraction. The inset corresponding to a blow-up of the dashed box shows a blow-up of the region between gratings 2 and 3 providing the information on the SPP contribution of the gratings and the constriction (see text).

relation (with $d_{1,2}$ the distance between gratings 1 and 2):

$$I_{1,3} = I_{2,3} \exp(-d_{1,2}/l). \tag{1}$$

Here $I_{1,3}$ ($I_{2,3}$) denotes the intensity measured at grating 1 (2) when illuminating at grating 3. Solving this equation yields a decay length $l = (11.7 \pm 3.3)\,\mu$m. This can be considered as a lower limit of the decay length as we neglect the enhanced losses in the gratings [29]. Furthermore, we analyse the emitted intensities at gratings 2 and 3 upon illumination of grating 1, now taking into account the presence of the MPC between gratings 2 and 3. As the

Table 1. Outcoupled intensities (in the same arbitrary units in both lines) for two positions of excitation (gratings 1 and 3) at the same input power. The background is subtracted.

Intensity (arb. u.)	Grating 1	Grating 2	Constriction	Grating 3
Excitation at grating 1	–	78.4	16.3	13.6
Excitation at grating 3	11.3	42.8	–	–

width of the constriction in the vicinity of the MPC is small compared to the SPP wavelength, the constriction acts as an effective barrier for the SPPs described by a transmission probability $0 < T_c < 1$. This is according to observations in [10, 11], where it was shown that the transmission drastically decreases at a threshold width of roughly 3 μm for the same wavelength and our own FDTD simulations (see SD (available from stacks.iop.org/NJP/15/113014/mmedia)). The intensity $I_{3,1}$ measured at grating 3 when illuminating grating 1 is related to the intensity $I_{2,1}$ measured at grating 2 when illuminating at grating 1 via

$$I_{3,1} = I_{2,1} \exp - ((d_{2,3} - 2.5\,\mu\text{m})/l)T_c. \tag{2}$$

Here, the effective distance $d_{2,3}$ is reduced by the length of the constriction to only account for the decay along the strip with constant width. Using l from above, we obtain the transmission probability as $T_c = (46 \pm 23)\%$. The relatively large error takes into account a linear error progression when assuming an uncertainty of 10% for the measured intensities and of 0.2 μm for the distances. Equivalent investigations were performed when the sample was bent with the help of the MCBJ mechanism, thus reducing the width of the contact in the centre of the constriction. We studied the situation in the tunnel regime, i.e. when the metal stripe is broken at the constriction and forms a few-atom contact. These studies are summarized in the SD. We found no systematic dependence of the SPP signals on the dc conductance of the contact, ranging from a few MΩ to several 10 Ω. This finding clearly shows that the dc conductance is to first order irrelevant for the coupling of the optoelectronic properties of metallic nanostructures. The average transmission over all situations amounts to 47%.

The value for the decay length is in reasonable agreement with findings of other groups [10, 11, 30]. Lamprecht *et al* showed that for a 70 nm thick but wide gold film, the decay length at a wavelength of 780 nm is about 40 μm. They found an additional damping mechanism when the stripe width is below 20 μm. In particular, they found the decay length of the SPPs on a stripe with a width of about 4 μm to be about one-third of the decay length of the SPPs measured on a wide film. As reported in [10, 11], the damping mechanism due to the finite width of a stripe sets in at values of a few micrometres. Zia *et al* [10] found an SPP decay length of 17 μm on a 48 nm thick gold stripe with a width of 4 μm when measuring at 780 nm. In contrast to these reports, we excite directly the SPPs within the restricted stripe and therefore the decay length might be slightly different.

To the best of our knowledge, the transmission of SPPs via long and narrow constrictions has not been studied quantitatively before. Nevertheless, one might expect a quite low transmission because the dimensions of the constriction with a length of 2.5 μm and a width of 20 nm up to 1 μm are well below the cut-off width of roughly 3 μm as measured by photon scanning tunnelling microscope studies reported in [10, 11].

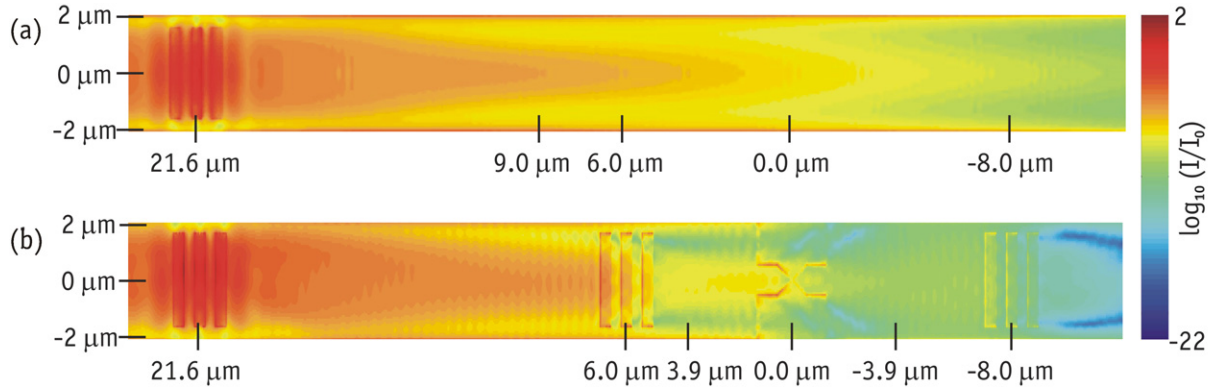

Figure 4. (a) Simulated intensity distribution for the excitation at one grating on a logarithmic scale. The markers at 6.0, 0 and $-8.0\,\mu$m represent the positions of the two gratings and the constriction in the actual sample design. The marker at $9.0\,\mu$m represents the position of the cross section shown in the SD. (b) Simulated intensity distribution for the excitation at grating 1 on a logarithmic scale for the actual sample design.

Strong near-field interaction of Au nanoparticle chains has been reported in [22, 23, 31–34] and has been interpreted as plasmon tunnelling. We attribute the surprisingly high transmission probability observed here to a similar coupling mechanism between the two sides of the constriction. While in the nanoparticle chain devices the individual particles are electrically isolated, the two sides of the constriction may be in good dc electrical contact in our experiment. Since the lateral dimensions of the constriction are well below the SPP wavelength, it does however act as tunnel barrier, regardless of the dc conductance. Due to the small width of the constriction, field enhancement effects may play a major role in the SPP transmission [4–7]. An alternative explanation could include the adiabatic transformation of the SPPs into localized SPPs at the apex of the constriction and their coupling to the other side [5, 35, 36]. Our present setup, however, does not allow discerning between these models.

To probe the model of field enhancement, we performed FDTD simulations (see also the SD (available from stacks.iop.org/NJP/15/113014/mmedia)). All simulations were done for a stripe made of gold on top of a polyimide layer and suspended in the constriction area as in the experiment and with the actual dimensions and the conditions of the optical setup used in the experiments. We started with a bare stripe carrying only one grating. The parameters of the grating are identical to the design parameters of the gratings used in the experiment.

Figure 4(a) depicts the intensity distribution (proportional to the square of the electric field E) at the surface of the sample gained from FDTD simulations. At variance to the real sample, in the simulations, we first assumed perfectly flat layers and perfectly sharp edges. We then repeated our simulations with a randomly distributed roughness of the gold of 5 nm (root mean square). The value of the roughness is gained from AFM measurements. This roughness did not affect the results. The shape of the edges which might be of importance is, however, not yet included in the simulations.

We evaluate the lateral intensity profile for determining the decay length of the SPPs. We average the intensity over cross sections taken at many distances and plot them as a function of distance (see SD for more details). The result is shown in figure 5. As the gratings 1 and 2 in

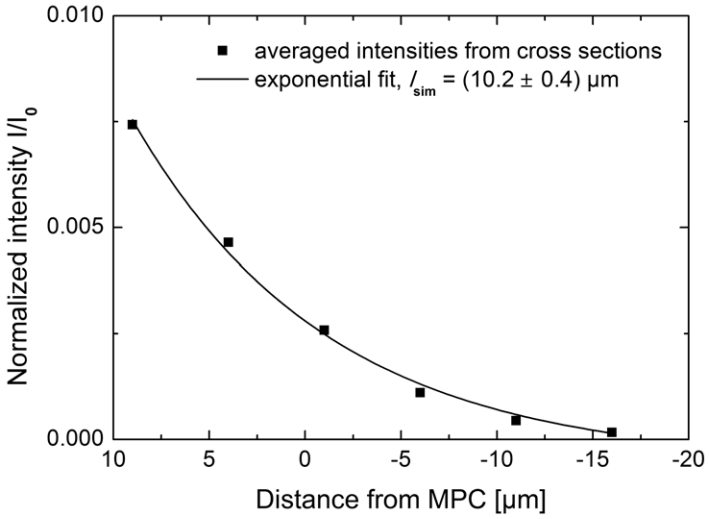

Figure 5. Averaged intensities from the simulated cross sections for the SPP excitation on the bare stripe carrying only one grating; the decay length of 10.2 μm is in good agreement with the experimental value. The data are normalized to the incident intensity.

the experiment are more than 14 μm away from the point of excitation, we start analysing the decay of SPPs at this distance in the simulation as well. We then calculate the decay length by fitting the values with an exponential decay and find $l_{\mathrm{sim}} = (10.2 \pm 1.2)\ \mu$m in good agreement with the experimentally determined value.

To complete the comparison between the experimental and numerical results, we performed FDTD simulations for the actual sample design including the gratings and the constriction. We show the results in figure 4(b), for the excitation at grating 1 which has a small step-like structure inside the trenches. Because of this step, the symmetry of the system is broken and the intensity profile along the stripe is not perfectly symmetric.

Figure 4(b) depicts the intensity distribution (proportional to $|E|^2$) at the surface of the sample gained from FDTD simulations. The constriction was designed to have a perfectly triangular shape. The simulation was performed for contact areas of the constriction at the narrowest part of 20×20 and $100 \times 100\,\mathrm{nm}^2$ in length and width, respectively. Again, we assumed perfectly flat layers and perfectly sharp edges. The intensity distribution is now superimposed by standing-wave patterns originating from reflected SPPs at the other gratings and at the constriction.

Figure 4(b) shows that SPP intensity is transmitted over the constriction towards grating 3, although the implemented cross section is well below the introduced cut-off-width of 3 μm reported earlier [10, 11]. Analogous to the determination of the decay length l_{sim}, we extract now the transmission probability $T_{\mathrm{c,sim}}$ from cross sections located at 3.9 and $-3.9\ \mu$m distance from the MPC (see figure 4(b)):

$$I_{(-3.9)} = I_{3.9} \exp\left(-\left(7.8\,\mu\mathrm{m} - 2.5\,\mu\mathrm{m}\right)/l_{\mathrm{sim}}\right) T_{\mathrm{c,sim}}. \tag{3}$$

From the travelling distance of 7.8 μm the length of the constriction of 2.5 μm is subtracted. Using l_{sim} from above, we find the transmission probabilities $T_{\mathrm{c,sim,100}} = (27 \pm 2)\%$ and $T_{\mathrm{c,sim,20}} = (58 \pm 2)\%$. Further simulations were performed investigating the transmission

of SPPs depending on the size of the contact area (see also the SD (available from stacks.iop.org/NJP/15/113014/mmedia)). For decreasing contact areas from 50×50 to $20 \times 20\,\mathrm{nm}^2$, we found an increase in the transmission. This finding points to emerging field enhancement effects caused by the smallness of the constriction [4–7]. The simulation results support the interpretation that the SPPs provide a strong coupling between the electronic systems of both sides of the constriction, despite their small width well below the SPP wavelength. The exact intensity distribution at the constriction and the gratings is obviously a result of a complex interplay of the incoming, transmitted and reflected SPPs at the edges of the gold stripe, the gratings and the constriction, respectively, as figure S7 in the SD indicates. The experimentally obtained transmission value fits well into the range set by the simulations, suggesting that the contact area in our experiments was in the range between 50×50 and $20 \times 20\,\mathrm{nm}^2$.

4. Conclusion

In conclusion, we showed in experiment and simulation that SPPs which are excited by grating couplers directly in a gold stripe and travel along the stripe have a shortened decay length compared to an infinite gold film. Furthermore, for the first time, we experimentally got access to the SPP intensity transmission across a constriction. We found a high transmission probability although the SPPs travel along a rather long constriction with lateral dimensions well below the wavelength of the SPPs. High transmission values are also observed when the sample is opened to form a few-atom contact or even a tunnel contact, showing that SPP transport is independent of dc coupling. This finding is important for the application of SPP transport in optoelectronic devices.

Acknowledgments

We thank A Erbe, S Juodkazis, H Misawa, K Ueno and R Waitz for valuable and fruitful discussions for this work. We acknowledge the experimental and technical assistance of M Bädicker, J C Berres, S Dickreuter, A Ganser and M Hagner. We gratefully acknowledge financial support from the Deutsche Forschungsgemeinschaft through SFB767 and the Strategic Japanese-German Cooperative Program of the JST and DFG on Nanoelectronics, from the Ministry of Science and Arts Baden-Württemberg through the Center of Applied Photonics and the Baden-Württemberg-Stiftung in the framework of the Research Network Functional Nanostructures.

References

[1] Zia R, Schuller J A, Chandran A and Brongersma M L 2006 *Mater. Today* **9** 20–7
[2] Ozbay E 2006 *Science* **311** 189–93
[3] Schuller J A, Barnard E S, Cai W, Jun Y C, White J S and Brongersma M L 2010 *Nature Mater.* **9** 193–205
[4] Ropers C, Neacsu C C, Elsaesser T, Albrecht M, Raschke M B and Lienau C 2007 *Nano Lett.* **7** 2784–88
[5] Schmidt S, Piglosiewicz B, Sadiq D, Shirdel J, Lee J S, Vasa P, Park N, Kim D-S and Lienau C 2012 *ACS Nano* **6** 6040–48
[6] Berweger S, Atkin J M, Xu X G, Olmon R L and Raschke M B 2011 *Nano Lett.* **11** 4309–13
[7] Berweger S, Atkin J M, Olmon R L and Raschke M B 2012 *J. Phys. Chem. Lett.* **3** 945–52

[8] Radko I P, Volkoy V S, Beermann J, Evlyukhin A B, Sondergaard T, Boltasseva A and Bozhevolnyi S I 2009 *Laser Photon. Rev.* **3** 575–90
[9] Heeres R W, Dorenbos S N, Koene B, Solomon G S, Kouwenhoven L P and Zwiller V 2010 *Nano Lett.* **10** 661–4
[10] Zia R, Schuller J A and Brongersma M L 2006 *Phys. Rev.* B **74** 165415
[11] Weeber J-C, Krenn J R, Dereux A, Lamprecht B, Lacroute Y and Goudonnet J P 2001 *Phys. Rev.* B **64** 045411
[12] Weeber J-C, Lacroute Y and Dereux A 2003 *Phys. Rev.* B **68** 115401
[13] Weeber J-C, Gonzalez M U, Baudrion A-L and Dereux A 2005 *Appl. Phys. Lett.* **87** 221101
[14] Guhr D C, Rettinger D, Boneberg J, Erbe A, Leiderer P and Scheer E 2007 *Phys. Rev. Lett.* **99** 086801
[15] Guhr D C, Rettinger D, Boneberg J, Erbe A, Leiderer P and Scheer E 2008 *J. Microsc.* **229** 407–14
[16] Ittah N, Noy G, Yutsis I and Selzer Y 2009 *Nano Lett.* **9** 1615–20
[17] Ittah N and Selzer Y 2011 *Nano Lett.* **11** 529–34
[18] Kolloch A, Benner D, Bädicker M, Waitz R, Geldhauser T, Boneberg J, Leiderer P and Scheer E 2011 *Proc. SPIE* **8204** 820404
[19] Ward D R, Hüser F, Pauly F, Cuevas J C and Natelson D 2010 *Nature Nanotechnol.* **5** 732–6
[20] Shi S-F, Xiaodong X, Ralph D C and McEuen P L 2011 *Nano Lett.* **11** 1814–18
[21] Prangsma J C, Kern J, Knapp A G, Grossmann S, Emmerling M, Kamp M and Hecht B 2012 *Nano Lett.* **12** 3915–19
[22] Savage K J, Hawkeye M M, Esteban R, Borisov A G, Aizpurua J and Baumberg J J 2012 *Nature* **491** 574–7
[23] Wu L, Duan H, Bai P, Bosman M, Yang J K W and Li E 2013 *ACS Nano* **7** 707–16
[24] Van Wijngaarden J T, Verhagen E, Polman A, Ross C E, Lezec H J and Atwater H A 2006 *Appl. Phys. Lett.* **88** 221111
[25] Radko I P, Bozhevolnyi S I, Brucoli G, Martin-Moreno L, Garcia-Vidal F J and Boltasseva A 2008 *Phys. Rev.* B **78** 115115
[26] Wang B, Aigouy L, Bourhis E, Gierak J, Hugonin J P and Lalanne P 2009 *Appl. Phys. Lett.* **94** 011114
[27] Lalanne P, Hugonin J P, Liu H T and Wang B 2009 *Surf. Sci. Rep.* **64** 453–69
[28] Léveque G and Martin O J F 2006 *J. Appl. Phys.* **100** 124301
[29] Kim D S, Hohng S C, Malyarchuk V, Yoon Y C, Ahn Y H, Yee K J, Park J W, Kim J, Park Q H and Lienau C 2003 *Phys. Rev. Lett.* **91** 143901
[30] Lamprecht B, Krenn J R, Schider G, Ditlbacher H, Salerno M, Felidj N, Leitner A and Aussenegg F R 2001 *Appl. Phys. Lett.* **79** 51–3
[31] Krenn J R, Salerno M, Felidj N, Lamprecht B, Schider G, Leitner A, Aussenegg F R, Weeber J-C, Dereux A and Goudonnet J P 2000 *J. Microsc.* **202** 122–8
[32] Maier S A, Kik P G and Atwater H A 2002 *Appl. Phys. Lett.* **81** 1714
[33] Chen H-Y, He C-L, Wang C-Y, Lin M-H, Mitsui D, Eguchi M, Teranishi T and Gwo S 2001 *ACS Nano* **5** 8223–29
[34] Denkova D, Verellen N, Silhanek A, Valev V K, Van Dorpe P and Moshchalkov V V 2013 *ACS Nano* **4** 3168–76
[35] Stockman M I 2004 *Phys. Rev. Lett.* **93** 137404
[36] Verhagen E, Spasenovic M, Polman A and Kuipers L 2009 *Phys. Rev. Lett.* **102** 203904